European Journal of Environmental and Civil Engineering

Taylor & Francis
Taylor & Francis Group

European Journal of Environmental and Civil Engineering

ISSN: (Print) (Online) Journal homepage: https://www.tandfonline.com/loi/tece20

A simplified approach to estimate settlements of earth embankments on piled foundations: the role of pile shaft roughness

Luca Flessati, Claudio di Prisco, Matteo Corigliano & Viviana Mangraviti

To cite this article: Luca Flessati, Claudio di Prisco, Matteo Corigliano & Viviana Mangraviti (2022): A simplified approach to estimate settlements of earth embankments on piled foundations: the role of pile shaft roughness, European Journal of Environmental and Civil Engineering, DOI: 10.1080/19648189.2022.2035259

To link to this article: https://doi.org/10.1080/19648189.2022.2035259

Published online: 10 Feb 2022.

EUROPEAN JOURNAL OF ENVIRONMENTAL AND CIVIL ENGINEERING
https://doi.org/10.1080/19648189.2022.2035259

A simplified approach to estimate settlements of earth embankments on piled foundations: the role of pile shaft roughness

Luca Flessati, Claudio di Prisco, Matteo Corigliano and Viviana Mangraviti

Dipartimento di Ingegneria Civile ed Ambientale, Politecnico di Milano, Milan, Italy

ABSTRACT

The use of piles as settlement reducers in the design of artificial embankments on soft soil strata is nowadays very common. The design methods employed in the current engineering practice are based on simplified approaches not allowing the assessment of average and differential settlements at the top of the embankment. In this paper, a model to estimate both differential and average displacements at the top of the embankment is introduced. This, based on the choice of substructuring the spatial domain and employing a suitably conceived upscaling procedure, is an extension to the case of rough pile shafts of a model originally conceived by the authors for smooth piles. To conceive and calibrate the model, the authors performed a series of numerical simulations mainly aimed at highlighting the mechanical processes taking place at the pile shaft. From a practical point of view, this model can fruitfully be employed in displacement based design approaches and to optimize pile diameter and spacing.

ARTICLE HISTORY
Received 24 April 2021
Accepted 24 January 2022

KEYWORDS
Piled-embankment; displacement based design; macroelement modelling

1. Introduction

A common technique adopted to reduce settlements in artificial embankments on soft soil strata is the employment of piles.

The mechanical response of these 'geo-structures' is commonly studied by analysing the stress redistribution taking place within the embankment, usually named 'arching effect'. In the past, numerous theoretical arching mechanisms (Carlsson, 1987; Chen et al., 2008; Collin, 2004; Handy, 1985; Hewlett & Randolph, 1988; Kempfert et al., 2004; Marston & Anderson, 1913; McKelvey, 1994; Rogbeck et al., 1998; Russell & Pierpoint, 1997; Svanø et al., 2000; Terzaghi, 1943; Van Eekelen et al., 2013; Zaeske, 2001) were proposed. The employment of some of these mechanisms is also suggested by the most used design standards (e.g. ASIRI, 2012; BS8006-1, 2010; CUR 226, 2010; EBGEO, 2010). All these approaches, disregarding the stiffness of the elements constituting the system, do not allow the assessment the embankment settlements.

The arching effect was also experimentally studied by performing trapdoor tests (Dewoolkar et al., 2007; Iglesia, 1991; Ladanyi & Hoyaux, 1969; Terzaghi, 1936; Vardoulakis et al., 1981). The experimental results put in evidence that, in contrast with what assumed by the previously cited theoretical models, the stress redistribution is significantly affected by the differential displacements imposed at the embankment base.

To take this effect into account, Iglesia et al. (1999, 2013) and King et al. (2017) introduced a 'Ground Reaction Curve', defining a relationship between differential settlement at the embankment base and

CONTACT Luca Flessati luca.flessati@polimi.it Dipartimento di Ingegneria Civile ed Ambientale, Politecnico di Milano, Piazza Leonardo da Vinci 32, Milano, 20133, Italy

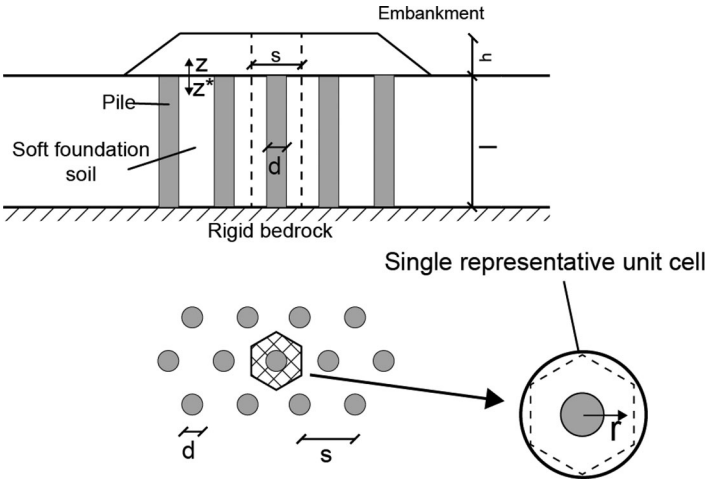

Figure 1. Geometry and definition of the single representative unit cell.

stress applied on the foundation soil. In a design perspective, this approach represents a first step toward a displacement-based design. However, the employment of this approach does not allow to calculate the displacements at the top of the embankment.

Recently, by interpreting the results of large series of numerical analysis, di Prisco et al. (2020a) introduced a new model, based on the sub-structuring of the spatial domain and on the concept of 'plane of equal settlements' (McGuire, 2011; McKelvey, 1994; Naughton, 2007; Terzaghi, 1943). The model is an incremental generalized constitutive relationship conceived in the framework of the macroelement approach, in which the progressively increasing embankment height is interpreted as a generalized loading variable, whereas both differential and average settlements at the embankment top are the output variables. The model is the result of a sort of upscaling procedure in which both geometry and local constitutive material response play, within the upscaled constitutive model, as the micro-mechanical grain interaction in the formulation/calibration of phenomenological constitutive models for geomaterials (Flessati et al., 2021; Pisanò et al., 2016). As is shown in Flessati (2021), the model proposed in di Prisco et al. (2020a) is a very convenient tool for designing the geometry (pile diameter and spacing) and assess the costs, once system performance (displacements) is fixed. The original model (di Prisco et al., 2020a) assumes: (i) pile shafts to be smooth, (ii) piles to be founded on a rigid bedrock and (iii) embankment construction to take place under drained conditions.

The ultimate goal of the research is the definition of a unique model for both piles founded on rigid bedrocks and floating piles, capable of taking into account pile shaft roughness and the consolidation process taking place in the foundation soil. In this direction, the authors have studied rough piles founded on a rigid bedrock and have extended the original model presented in di Prisco et al. (2020a). To this aim, the authors have performed a series of numerical finite difference (FD) numerical analyses by means of the commercial code FLAC 3 D (FLAC3D 7.0, Itasca Consulting Group Inc, 2017).

The paper is structured as it follows, in Section 2 the numerical analyses are presented, in Section 3 the new model is introduced, whereas in Section 4 the model is validated. Finally, in Section 5 a practical application of the proposed model is suggested.

2. Numerical analyses

The construction of an earth embankment on piled foundations is a complex three-dimensional problem with a geometry evolving during the construction phase. In case the transversal dimension of the embankment is large with respect to its height (Figure 1), in the preliminary dimensioning phase, flanks effects are disregarded and the problem is generally approached by considering one representative axisymmetric unit cell (Chen et al., 2008; di Prisco et al., 2020a, 2020b; Han & Gabr, 2002; Mangraviti et al., 2021; Plaut & Filz, 2010; Van Eekelen et al., 2011).

Table 1. Geometry.

d (m)	s (m)	l (m)	h_e (m)
0.5	1.5	5	5

The unit cell (Figure 1) of diameter s, assumed equal to the pile spacing (different values can be considered in case of different pile patterns) is composed by: (i) the pile (with diameter d and length l), (ii) a l-thick soft soil stratum and (iii) the embankment, characterized by a progressively increasing height h. The final embankment height is named h_e. Both the pile and the soft soil stratum are assumed to be positioned over a rigid bedrock.

The numerical analyses were performed by assuming drained conditions and by employing the numerical model described in di Prisco et al. (2020a). The pile is assumed to be elastic, whereas both foundation and embankment soil behaviour, analogously to what done by other authors (Abdullah & Edil, 2007; Ambily & Gandhi, 2007; Ariyarathne et al., 2013; Chen et al., 2008; Das & Deb, 2018; Han & Gabr, 2002; Han et al., 2007; Huang & Han, 2010; Lehn et al., 2016; Liu et al., 2007; Stewart & Filz, 2005; Wijerathna & Liyanapathirana, 2020; Yan et al., 2006; Yapage & Liyanapathirana, 2014; Zheng et al., 2019; Zhuang et al., 2020) is assumed to be elastic-perfectly plastic. The yield function is defined according to the Mohr-Coulomb failure criterion and the flow rule is assumed to be non-associated. Since the constitutive relationship, despite of its simplicity, is capable of capturing the main aspects of the mechanical processes taking place in the domain, the results obtained by employing more sophisticated constitutive relationships, for instance strain hardening elastic-plastic constitutive relationships, taking into account the development of irreversible strains from the initial phases of the loading process or the effect of induced anisotropy (e.g. Dafalias & Manzari, 2004; di Prisco et al., 1993; Manzari & Dafalias, 1997; Marveggio et al., 2022), are not expected to be qualitatively different. It is also worth mentioning that, for practical applications, sophisticated constitutive relationships, although more reliable in reproducing the material response, very often cannot be properly calibrated owing to the lack of a sufficient number of laboratory/in situ tests data.

The unique difference between the numerical model employed in this case and the one employed in di Prisco et al. (2020a) is the presence of rough interface elements between pile and foundation soil. Along normal direction, under compression, the interface elements are 'quasi rigid' (the elastic stiffness is sufficiently larger than the soil one), whereas under tension perfectly fragile. Along the tangential direction a 'quasi-rigid'-perfectly plastic behaviour, with a yield function defined according to the Mohr-Coulomb failure criterion and nil dilatancy, is assumed. The interface friction angle is hereafter named δ. The interface cohesion is imposed to be nil.

The layer-by-layer embankment construction is subdivided in single stages, each one corresponding with the deposition of 25 cm of compacted granular material (for the sake of simplicity, the on-site compaction process is not simulated). To reproduce, although in a simplified way, the real loading path followed by the system during the embankment construction, at each construction stage, a new stratum of elements is added on the (current position) of the embankment top.

The authors performed a parametric study; in this section, for the sake of clarity, one reference case is first discussed. The system geometry and the material mechanical properties are reported in Tables 1 and 2, respectively. The foundation soil-pile interface friction angle is assumed equal to 2/3 of the foundation soil one ($\delta = 20^\circ$).

2.1. Numerical results: global response

In this subsection the system response is analysed from a global perspective, in terms of displacements at both the embankment top and base and vertical stresses at the embankment base.

By following what suggested in di Prisco et al. (2020a), the global response is analysed by employing the following non-dimensional variables:

$$H = \frac{h}{d}, \tag{1}$$

$$U_{t,diff} = U_{t,f} - U_{t,c}, \tag{2}$$

Table 2. Constitutive model parameters and unit weights.

	Unit weight (kN/m^3)	Young modulus (MPa)	Poisson ratio (-)	Friction angle (°)	Cohesion (kPa)	Dilatancy angle (°)
Foundation soil	18	1	0.3	30	0	0
Embankment	18	10	0.3	40	0	0
Column	25	30000	0.3	–	–	–

$$U_{t,av} = \frac{U_{t,f}(S^2 - 1) + U_{t,c}}{S^2}, \tag{3}$$

$$U_{b,f} = \frac{u_{b,f}}{l}\frac{E_{oed,f}}{d\ \gamma_e}, \tag{4}$$

$$\Sigma_f = \frac{\sigma_f}{d\ \gamma_e}, \tag{5}$$

being $S = s/d$, $E_{oed,f}$ the foundation soil oedometric elastic modulus, γ_e the embankment soil unit weight, whereas $u_{b,f}$ and σ_f the average values of vertical displacement and vertical stresses for $z = 0$ (coordinate z is defined in Figure 1) and $d/2 < r < s/2$ (coordinate r is defined in Figure 1), respectively. The non-dimensional displacement variables $U_{t,c}$ and $U_{t,f}$ are defined as:

$$U_{t,c} = \frac{u_{t,c}}{l}\frac{E_{oed,f}}{d\ \gamma_e}, \tag{6}$$

$$U_{t,f} = \frac{u_{t,f}}{l}\frac{E_{oed,f}}{d\ \gamma_e}, \tag{7}$$

being $u_{t,c}$ and $u_{t,f}$ the average values of vertical displacement at the top of the embankment ($z = h$) for $0 < r < d/2$ and for $d/2 < r < s/2$, respectively.

As was suggested in di Prisco et al. (2020a), the employment of these non-dimensional variables is particularly convenient since, in the non-dimensional $U_{t,diff}$-H and $U_{t,av}$-H planes, the response is unique if the non-dimensional geometrical ratios (S, $L = l/d$), the non-dimensional stiffness ratio ($E_{oed,e}/E_{oed,f}$, being $E_{oed,e}$ the embankment soil oedometric modulus) and the embankment soil failure parameters (friction and dilatancy angle values, ϕ'_e and ψ_e, respectively) are kept constant.

The results relative to the reference case are plotted in Figure 2. In particular, the results are plotted in the $U_{t,diff}$-H, $U_{t,av}$-H, $U_{b,f}$-H and Σ_f-H planes in Figure 2(a–d), respectively. For the sake of clarity, in the same figures the results relative to the corresponding case in which $\delta = 0$ are plotted.

In Figure 2 it is evident that:

- displacements for the rough pile are smaller due to the development of shear stresses along the pile shaft;
- for $\delta = 0°$ the initial slope of all the non-dimensional displacement-height curves is one, implying no stress redistribution taking place (di Prisco et al., 2020a). On the contrary, for $\delta = 20°$ the initial slope is significantly smaller;
- the embankment height for which differential settlements stop increasing (H^*) is practically coincident in the two cases. H^* is the height of the plane of equal settlements;
- the final branches of $U_{t,av}$-H curves are parallel;
- $U_{b,f}$ is continuously increasing with H, meaning that a 'complete' arching mechanism, deviating all the vertical stresses coming from the embankment toward the pile, does not develop. According to di Prisco et al. (2020a), this is due to the embankment vertical deformability;
- Σ_f is slightly larger for $\delta = 20°$ (due to the non-nil interface friction the system is globally more rigid), even if $U_{b,f}$ is significantly different in the two cases.

2.2. Numerical results: local response

In case the roughness of the pile shaft is taken into consideration, during the embankment construction yielding takes place not only in the embankment, but also at the interface along the pile shaft.

The local mechanical response of the embankment is qualitatively coincident with the one obtained for smooth piles by di Prisco et al. (2020a), therefore, for the sake of brevity, the corresponding results

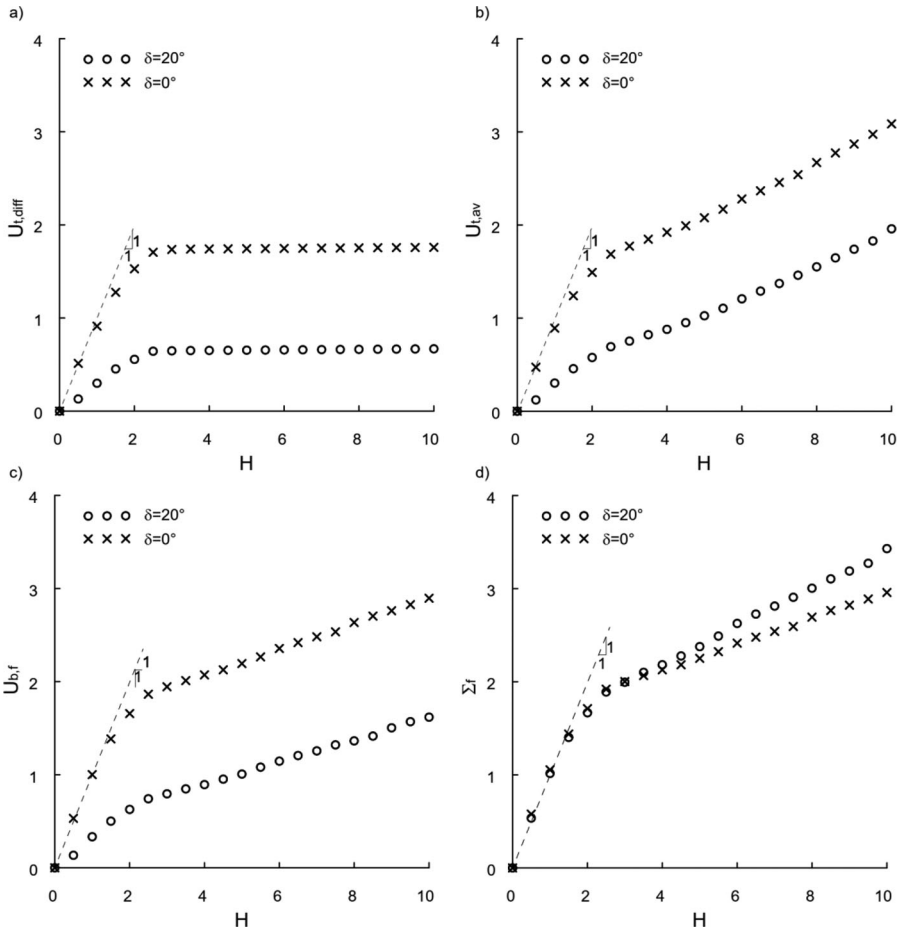

Figure 2. Variation with H of (a) $U_{t,diff}$, (b) $U_{t,av}$, (c) $U_{b,f}$ and (d) Σ_f for the reference case (Tables 1 and 2) and for the corresponding case with a smooth pile ($\delta = 0°$).

are hereafter omitted. However, for the sake of completeness, the main aspects of the embankment response are summarized here below:

- during the embankment construction, yielding takes place under simple shear conditions in a narrow crown ('process zone') of height $h_{p,e}$ (subscript e, absent in di Prisco et al. (2020a), stands for embankment) of soil located close to the pile top;
- $h_{p,e}$, initially coincident and evolving with h, stops increasing when a sufficiently large value of h is reached. The final value of $h_{p,e}$ coincides with the height of the plane of equal settlements.
- the embankment soil not belonging to the process zone is under pseudo-oedometric conditions and, according to the employed constitutive relationship, behaves elastically.

The numerical results highlighting the mechanical response of the foundation soil, markedly different with respect to the smooth shaft case, are summarized in Figures 3–6.

The evolutions with h of vertical stress (σ_v) profile along depth (z^*=-z) for $r = d/2$ (along pile-foundation soil interface) and for $r = s/2$ are plotted in Figure 3(a,b), respectively. For the sake of clarity, in Figure 3 some construction stages were omitted. For the sake of completeness, the dashed lines of Figure 3 represent the initial geostatic (i.e. $h = 0$) condition.

As is evident, an arching effect, deviating vertical stresses toward the pile, takes place in the foundation soil. The soil stratum at the bottom is practically unaffected by the construction process. The average inclination of initial branches of vertical stress distributions is progressively increasing with h. Owing to

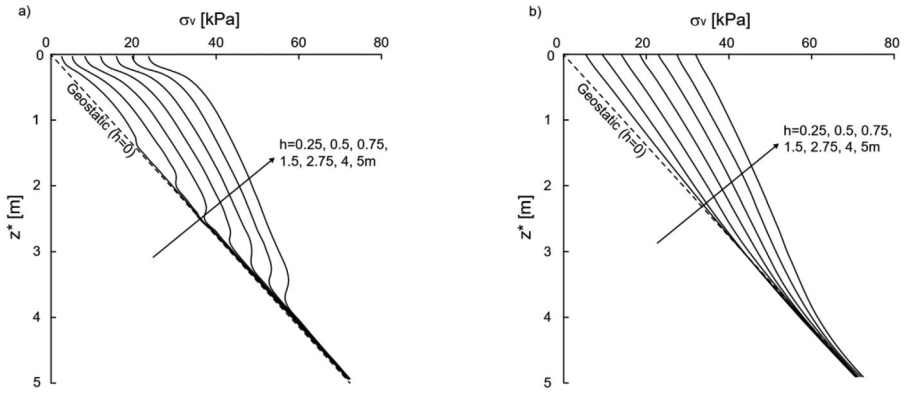

Figure 3. Variation along depth vertical stresses: (a) $r = d/2$ and (b) $r = s/2$.

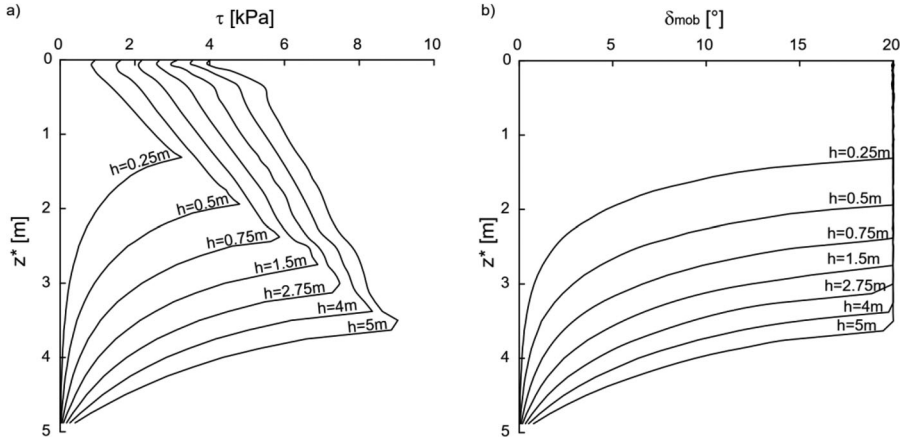

Figure 4. Variation along depth of: (a) τ and (b) δ_{mob}.

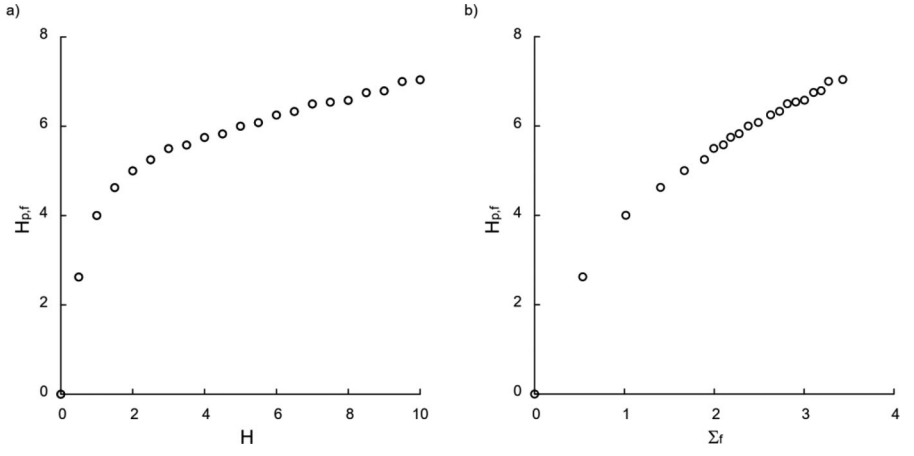

Figure 5. Evolution of $H_{p,f}$ with (a) H and (b) Σ_f.

presence of a rigid bedrock under the pile tip, for very large *h/d* ratio values, the vertical stress distribution is expected to be linearly decreasing with depth. However, this stress distribution has been obtained only for *h/d* ratio values not commonly adopted in practice. The corresponding results are hereafter omitted for the sake of brevity.

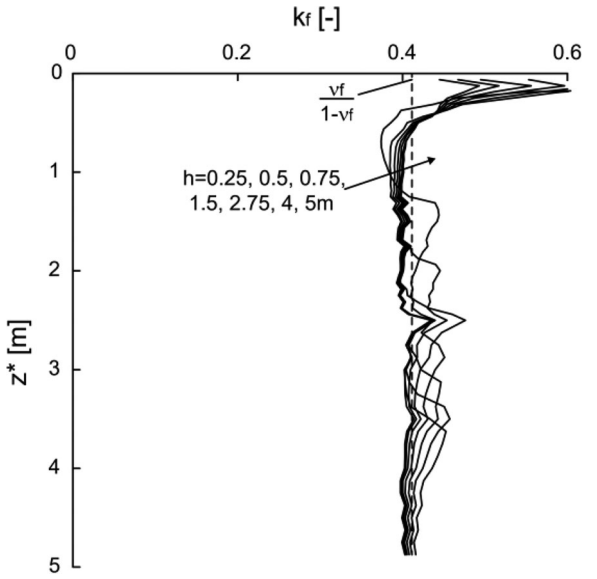

Figure 6. Variation along depth of k_f.

The trends of vertical stresses are very different with respect to smooth shaft case (not reported for the sake of brevity), since in the rough case a continuous along depth vertical stress migration toward the pile takes place. This observation is confirmed by the development of tangential stresses (τ) in the foundation soil. In Figure 4(a), only the distribution of τ with depth along the pile-foundation soil interface is plotted.

The tangential stress distributions along depth are characterized by two different branches. The linear one, close to the ground surface, is obtained where the interface is yielded (i.e. $\delta_{mob} = \delta$, being δ_{mob} the mobilized interface friction angle, as is shown in Figure 4(b)). The second parabolic one where the interface is not yet yielded (i.e. $\delta_{mob} < \delta$, as is shown in Figure 4(b)). The transition from one branch to the other is defined by a well pronounced peak.

The plastic height, i.e. vertical distance of the peak from the ground surface, hereafter named $h_{p,f}$, progressively increases with the embankment height as is shown in Figure 5(a), where the numerical results are plotted in the non-dimensional $H_{p,f}$-H plane, being $H_{p,f} = h_{p,f}/d$. For the sake of completeness, in Figure 5(b) the results are also plotted in the $H_{p,f}$-Σ_f plane. In Section 3 the evolution of $H_{p,f}$ is shown to be essential for the definition of the model capable of reproducing the system response.

Finally, for the sake of completeness, the variation along depth for $r = d/2$ of ratio of horizontal and vertical stress (k_f) is plotted in Figure 6. k_f is almost constant along depth and equal to the value expected in the elastic case ($k_f = \nu_f/(1\text{-}\nu_f)$, being ν_f the foundation soil Poisson's ratio), suggesting that tangential stresses developing at the pile-soil interface do not induce yielding in the surrounding foundation soil.

3. Generalized constitutive relationship

The model proposed in di Prisco et al. (2020a) is a generalized upscaled constitutive relationship conceived in the framework of the macroelement approach. The macroelement approach, commonly employed to analyse different soil structure interaction problems (e.g. shallow foundations (Cremer et al., 2002; Flessati et al., 2021; Gottardi et al., 1999; Grange et al., 2009; Montrasio & Nova, 1997; Nova & Montrasio, 1991; Pisanò et al., 2016), offshore foundations and wind turbines (Byrne & Houlsby, 2003; Cassidy et al., 2006; Martin & Houlsby, 2001), buried pipelines (Cocchetti et al., 2009), rock boulders impacting on granular soil strata (di Prisco & Vecchiotti, 2006), pile foundations (Li et al., 2016), anchored wire meshes (Boschi et al., 2020, 2021, 2022) tunnel cavities (di Prisco & Flessati, 2021a) and tunnel fronts (di Prisco et al., 2018, 2020c; Flessati & di Prisco, 2020), stems from the idea of (i) describing the mechanical response of a complex system by means of a low number of degrees of freedom and (ii) defining an

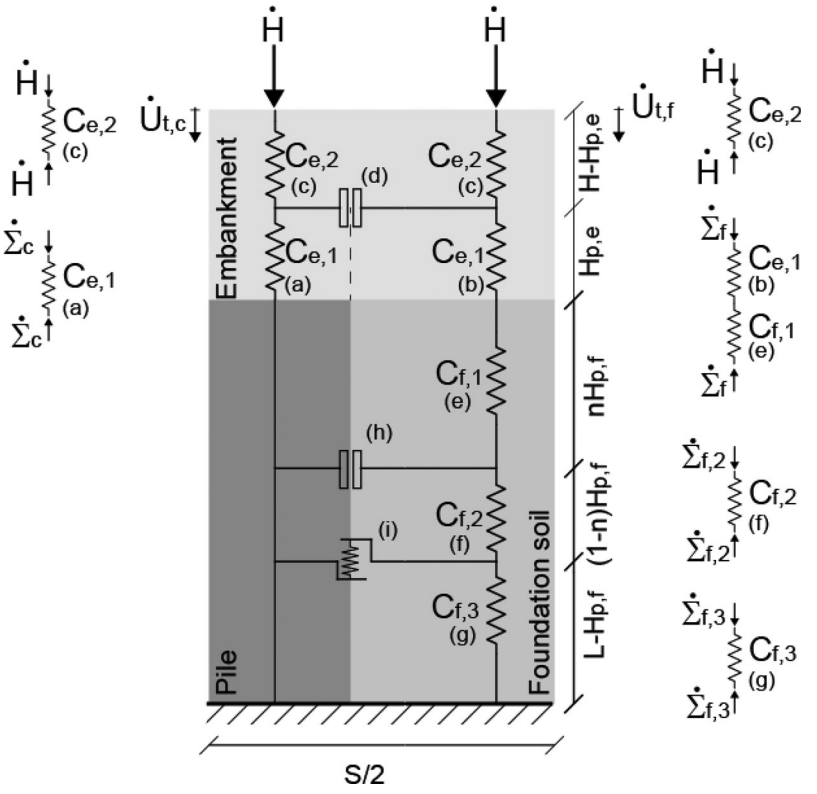

Figure 7. Rheological scheme.

upscaled constitutive law, relating the generalized static and kinematic variables associated with the chosen degrees of freedom.

For earth embankments on smooth piles, di Prisco et al. (2020a) propose to consider as degrees of freedom (i) the non-dimensional embankment height (to be interpreted as a generalized loading variable) and (ii) both non-dimensional differential and average displacements of the embankment top. The relationship between these variables is expressed as:

$$\begin{bmatrix} \dot{U}_{t,diff} \\ \dot{U}_{t,av} \end{bmatrix} = \begin{bmatrix} C_{diff} \\ C_{av} \end{bmatrix} \dot{H}, \tag{8}$$

where dots stands for increments, whereas the generalized non-dimensional compliances C_{diff} and C_{av} depend on (i) geometry, (ii) material properties and (iii) on $H_{p,e}$ ($H_{p,e} = h_{p,e}/d$), interpreted as a generalized hardening variable.

In contrast, when rough piles are considered, C_{diff} and C_{av} to take the arching effect developing in the foundation soil into account, must also depend on $H_{p,f}$.

To calculate the new expressions for C_{diff} and C_{av} the authors employed the rheological scheme, inspired to the one of di Prisco et al. (2020a), sketched in Figure 7.

The rheological scheme is composed by:

- two elastic springs ((a) and (b)) of compliance $C_{e,1}$, modelling the embankment for $z < h_{p,e}$ ((a) and (b), referring to $0 < r < d/2$ and $d/2 < r < s/2$, respectively);
- two elastic springs (c) of compliance $C_{e,2}$, modelling the embankment for $z > h_{p,e}$;
- a plastic slider (d), defining the stress redistribution in the embankment, modelling the stress transfer in the embankment process zone;
- three elastic springs ((e), (f) and (g)) of compliance $C_{f,1}$, $C_{f,2}$ and $C_{f,3}$, modelling the foundation soil;
- a plastic slider and an elastic shear spring ((h) and (i), respectively), modelling the stress transfer along the pile-foundation soil interface.

The pile is assumed to be rigid, but, by introducing additional springs, the model can easily be extended to the case of deformable piles.

The compliance of the springs modelling the embankment, coincident with the ones proposed in di Prisco et al. (2020a), can be expressed as:

$$C_{e,1} = \frac{H_{p,e}}{E_{oed,e}} \frac{E_{oed,f}}{L}, \tag{9}$$

$$C_{e,2} = \frac{H - H_{p,e}}{E_{oed,e}} \frac{E_{oed,f}}{L}. \tag{10}$$

These springs are non-linear and irreversible since their stiffness is not constant but evolving with both H and $H_{p,e}$ (geometrical and mechanical non-linearities).

For the plastic slider in the embankment, as is done in di Prisco et al. (2020a), a Mohr-Coulomb failure criterion is employed:

$$\dot{\mathcal{T}}_{p,e} = \dot{\mathcal{N}}_{p,e} \tan \phi'_{ss}, \tag{11}$$

being $\dot{\mathcal{T}}_{p,e}$ and $\dot{\mathcal{N}}_{p,e}$ the increments in the non-dimensional tangential and normal forces transferred throughout the (plastic) shear zone in the embankment (subscript e, absent in di Prisco et al., 2020a, stands for embankment), respectively, whereas ϕ'_{ss} is the friction angle of embankment soil under simple shear conditions (di Prisco & Flessati, 2021b; di Prisco & Pisanò, 2011; Drescher & Detournay, 1993; Vermeer, 1990):

$$\tan \phi'_{ss} = \frac{\cos \psi_e \sin \phi'_e}{1 - \sin \psi_e \sin \phi'_e}. \tag{12}$$

By following what suggested in di Prisco et al. (2020a), (i) vertical stresses along the process zone are assumed to be linearly increasing with depth according to a geostatic distribution and (ii) the ratio of horizontal and vertical stresses along the process zone (k_e) to be constant. Therefore:

$$\mathcal{N}_{p,e} = \frac{\int_0^{h_{p,e}} \gamma_e (h - z) \bar{k}_e d\pi dz}{\gamma_e d^3} = \pi \bar{k}_e H H_{p,e} - \pi \bar{k}_e \frac{H_{p,e}^2}{2} \tag{13}$$

being $\bar{k}_e$ the average value of k_e. By differentiating Equation (13) it reads:

$$\dot{\mathcal{N}}_{p,e} = \pi \bar{k}_e H_{p,e} \dot{H} + \pi \bar{k}_e (H - H_{p,e}) \dot{H}_{p,e}. \tag{14}$$

As is shown in di Prisco et al. (2020a), the simplifying assumption on the vertical stress distribution does not compromise the capability of the model of reproducing the numerical results.

As was previously mentioned and as was proposed by di Prisco et al. (2020a), $H_{p,e}$ has to be interpreted as a generalized hardening variable. Its evolution rule is expressed as it follows:

$$\dot{H}_{p,e} = \begin{cases} \dot{H} & \text{if } H < H^* \\ 0 & \text{if } H \geq H^* \end{cases}, \tag{15}$$

where, the value of H for which $H_{p,e}$ stops evolving is the height of the plane of equal settlements (H^*). H^* is not a constitutive parameter but is calculated by imposing $C_{diff} = 0$.

The compliance of springs modelling the foundation soil ((e), (f) and (g) of Figure 7) are expressed as:

$$C_{f,1} = \frac{n H_{p,f}}{E_{oed,f}} \frac{E_{oed,f}}{L} = \frac{n H_{p,f}}{L}, \tag{16}$$

$$C_{f,2} = \frac{(1-n) H_{p,f}}{E_{oed,e}} \frac{E_{oed,f}}{L} = \frac{(1-n) H_{p,f}}{L}, \tag{17}$$

$$C_{f,3} = \frac{L - H_{p,f}}{E_{oed,e}} \frac{E_{oed,f}}{L} = \frac{L - H_{p,f}}{L}, \tag{18}$$

where the non-dimensional coefficient n defines the position of the plastic slider (h) of Figure 7, for which a Mohr-Coulomb failure criterion is adopted:

$$\dot{\mathcal{T}}_{p,f} = \dot{\mathcal{N}}_{p,f} \tan \delta, \tag{19}$$

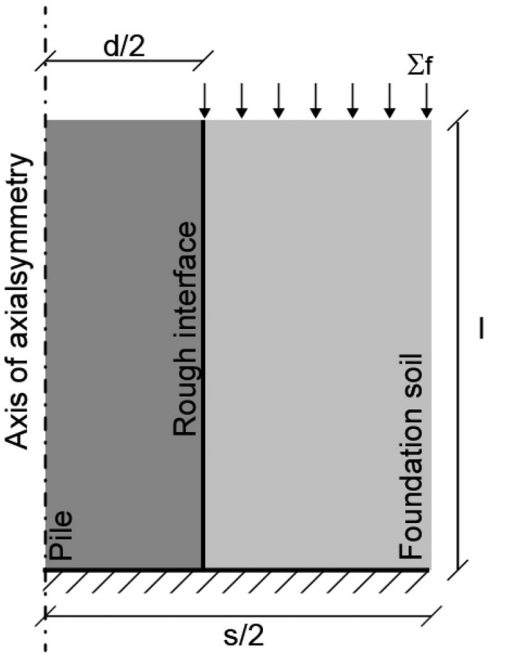

Figure 8. Geometry considered for the numerical analyses ($d = 0.5$ m, $S = 2$, 3, 4, 5, 7 and $L = 6$, 10, 16, 24, 40).

being $\dot{\mathcal{T}}_{p,f}$ and $\dot{\mathcal{N}}_{p,f}$ the increments in the non-dimensional tangential and normal forces transferred throughout the yielded portion of the interface. Analogously to what done for the process zone in the embankment (Equation (13)), to calculate $\mathcal{N}_{p,f}$ the authors assumed a constant value of k_f along the yielded part of the pile-soil interface (Figure 6) and a linear distribution for vertical stresses:

$$\sigma_v(z^*) = \sigma_f + \gamma_f z^* \tag{20}$$

being γ_f the foundation soil unit weight. Under these assumptions:

$$\mathcal{N}_{p,f} = \frac{\int_0^{h_{p,f}} (\sigma_f + \gamma_f z^*) \bar{k}_f d\pi dz^*}{\gamma_e d^3} = \pi \bar{k}_f \left(\Sigma_f H_{p,f} + \frac{1}{2} \frac{\gamma_f}{\gamma_e} H_{p,f}^2 \right) \tag{21}$$

and consequently

$$\dot{\mathcal{N}}_{p,f} = \pi \bar{k}_f \left[H_{p,f} \dot{\Sigma}_f + \left(\Sigma_f + \frac{\gamma_f}{\gamma_e} H_{p,f} \right) \dot{H}_{p,f} \right], \tag{22}$$

being $\bar{k}_f$ the average value of k_f along the yielded part of the pile-soil interface and, by imposing the balance of momentum along the vertical direction:

$$\dot{\Sigma}_f = \left(1 - \frac{4 \tan \phi_{ss}' \bar{k}_e}{S^2 - 1} H_{p,e} \right) \dot{H}. \tag{23}$$

The simplified vertical stress distribution assumed by the model (Equation (20)) does not coincide with the numerical one (Figure 3). However, this simplifying assumption, reasonable for not too large embankments height values ($H < 10$), does not compromise the model capability of reproducing the system response (Section 3.3).

For the sake of simplicity, to calculate the non-dimensional force ($\mathcal{T}_{e,f}$), associated with the elastic shear spring (element (i) of Figure 7), a parabolic distribution for tangential stresses (Figure 4(a)) is assumed:

$$\mathcal{T}_{e,f} = \frac{1}{3} \pi \bar{k}_f \tan \delta \left(\Sigma_f + \frac{\gamma_f}{\gamma_e} H_{p,f} \right) (L - H_{p,f}) \tag{24}$$

corresponding to:

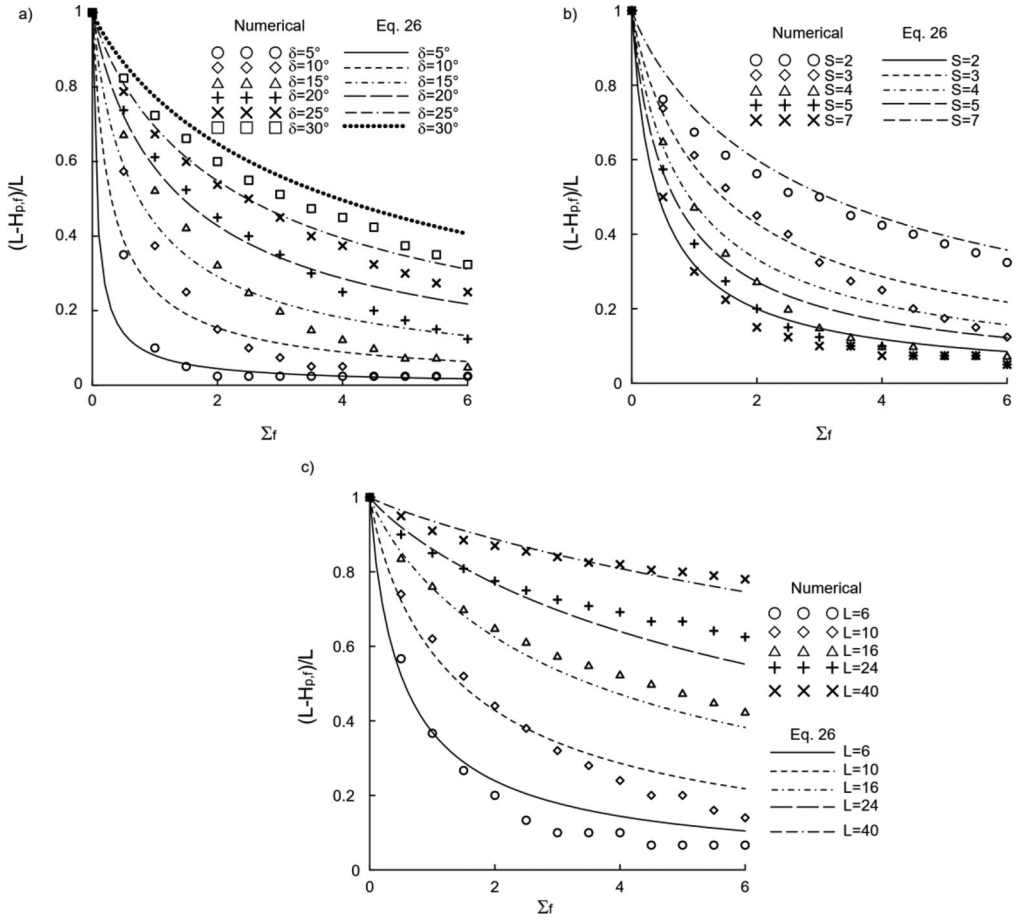

Figure 9. Variation of $H_{p,f}$ with Σ_f: (a) for different δ values, (b) for different S values and (c) for different L values.

$$\dot{\mathcal{T}}_{e,f} = \frac{1}{3}\pi \bar{k}_f \tan\delta \left\{ (\mathrm{L} - \mathrm{H_{p,f}}) \left(1 - \frac{4\tan\phi'_{ss}\bar{k}_e}{S^2 - 1} H_{p,e} \right) \dot{H} + \left[\frac{\gamma_f}{\gamma_e} (\mathrm{L} - 2H_{p,f}) - \Sigma_f \right] \dot{H}_{p,f} \right\} \tag{25}$$

As is evident from Equations (19), (22), and (25), the increase in the transferred shear forces depends on both loading variable $\dot{H}$ and increment of the generalized hardening variable $H_{p,f}$. Its evolution rule is defined in Section 3.1.

3.1. Definition of $H_{p,f}$ evolution

For the sake of simplicity, to derive the evolution rule for $H_{p,f}$, the mechanical problem illustrated in Figure 8, where Σ_f is the controlled variable, is numerically solved by means of FD analyses.

Even in this case, the interface between pile and foundation soil is assumed to be rough, the pile to be elastic and the foundation soil to be elastic-perfectly plastic (the failure criterion is given by the Mohr-Coulomb criterion and the flow rule is assumed to be non-associated). The values of material parameters are the one of the reference case (Table 2).

The authors performed a parametric study by considering different values of δ, S and L. The corresponding numerical results are plotted in Figure 9 in the $(L\text{-}H_{p,f})/L\text{-}\Sigma_f$ plane.

Table 3. Values of interpolating parameters.

h_1	h_2	h_3	h_4
0.4	1.7	1.95	0.9

The numerical results were interpolated by means of the following expression:

$$\frac{L-H_{p,f}}{L} = \frac{h_1 L^{h_2}\tan^{h_3}\delta}{(S-1)\Sigma_f^{h_4} + h_1 L^{h_2}\tan^{h_3}\delta}, \tag{26}$$

where h_1, h_2, h_3 and h_4 are non-dimensional parameters. The curves obtained by employing the values of h_1, h_2, h_3 and h_4 reported in Table 3 are plotted in Figure 9. As is evident, the agreement is satisfactory.

By differentiating Equation (26) and by using Equation (23), the following expression:

$$\dot{H}_{p,f} = \frac{(S-1)h_1\ L^{h_2+1}\tan^{h_3}\delta h_4 \Sigma_f^{h_4-1}}{\left[(S-1)\Sigma_f^{h_4} + h_1 L^{h_2}\tan^{h_3}\delta\right]^2}\left(1 - \frac{4\bar{k}e\tan\phi'_{ss}H_{p,e}}{S^2-1}\right)\dot{H} = f_1\dot{H}, \tag{27}$$

is obtained.

3.2. Non-dimensional compliance definition

By imposing (i) the balance of momentum along the vertical direction, (ii) compatibility conditions, (iii) constitutive relationships for all the elements (Appendix A) and by using the generalized hardening rules (Equations (15) (23), and (27)) we obtain:

$$\begin{aligned} C_{diff} = &\left[\left(1 - \frac{4\tan\phi'_{ss}\bar{k}_e H_{p,e}}{S^2-1}\right)C_{f,1} - \frac{4S^2\tan\phi'_{ss}\bar{k}_e H_{p,e}}{S^2-1}C_{e,1}\right] \\ &+ \left\langle\left(1 - \frac{4\tan\phi'_{ss}\bar{k}_e H_{p,e}}{S^2-1}\right)\left(1 - \frac{4\tan\delta\bar{k}_f H_{p,f}}{S^2-1}\right) - \frac{4\bar{k}_f\tan\delta}{S^2-1}\left(\Sigma_f + \frac{\gamma_f}{\gamma_e}H_{p,f}\right)f_1\right\rangle C_{f,2} \\ &+ \left\langle\left(1 - \frac{4\tan\phi'_{ss}\bar{k}_e H_{p,e}}{S^2-1}\right)\left(1 - \frac{4\tan\delta\bar{k}_f (L+2H_{p,f})}{3(S^2-1)}\right) - \frac{4\bar{k}_f\tan\delta}{3(S^2-1)}\left[2\Sigma_f + \frac{\gamma_f}{\gamma_e}(L+H_{p,f})\right]f_1\right\rangle C_{f,3}, \end{aligned} \tag{28}$$

$$\begin{aligned} C_{av} = &C_{e,1} + C_{e,2} + \left(1 - \frac{4\tan\phi'_{ss}\bar{k}_e H_{p,e}}{S^2-1}\right)\left(\frac{S^2}{S^2-1}\right)C_{f,1} \\ &+ \left(\frac{S^2}{S^2-1}\right)\left\langle\left(1 - \frac{4\tan\phi'_{ss}\bar{k}_e H_{p,e}}{S^2-1}\right)\left(1 - \frac{4\tan\delta\bar{k}_f H_{p,f}}{S^2-1}\right) - \frac{4\bar{k}_f\tan\delta}{S^2-1}\left(\Sigma_f + \frac{\gamma_f}{\gamma_e}H_{p,f}\right)f_1\right\rangle C_{f,2} \\ &+ \left(\frac{S^2}{S^2-1}\right)\left\langle\left(1 - \frac{4\tan\phi'_{ss}\bar{k}_e H_{p,e}}{S^2-1}\right)\left(1 - \frac{4\tan\delta\bar{k}_f (L+2H_{p,f})}{3(S^2-1)}\right) - \frac{4\bar{k}_f\tan\delta}{3(S^2-1)}\left[2\Sigma_f + \frac{\gamma_f}{\gamma_e}(L+H_{p,f})\right]f_1\right\rangle C_{f,3} \end{aligned} \tag{29}$$

3.4. Model calibration

Ten are the model input data to be assigned, 3 referring to geometry (d, s and l), 4 to embankment soil mechanical properties ($E_{oed,e}$, ϕ'_e, ψ_e, and γ_e), 2 to foundation soil mechanical properties ($E_{oed,f}$ and γ_e) and 1 to pile-foundation soil interface (δ).

The model has 3 constitutive parameters: $\bar{k}_e$, $\bar{k}_f$ and n.

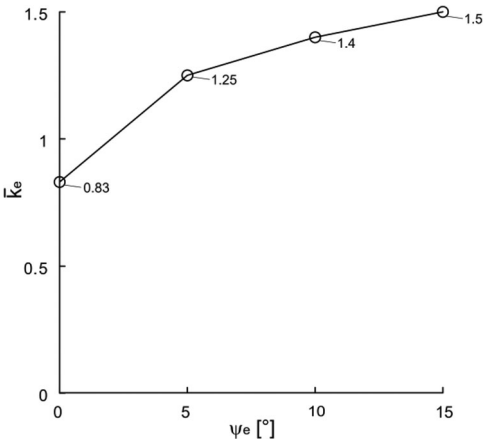

Figure 10. Variation of $\bar{k}_e$ with ψ_e (di Prisco et al., 2020a).

As was previously mentioned (Section 2.2), the local embankment response is not significantly affected by the pile shaft roughness. For this reason, by following what suggested in di Prisco et al. (2020a), $\bar{k}_e$ is assumed to be dependent only on the embankment soil dilatancy angle, as is shown in Figure 10.

As is suggested by Figure 6, $\bar{k}_f$ is assumed to be equal to $\nu_f/(1\text{-}\nu_f).n$ (Equations (16) and (17)) defines the position of plastic slider (h) of Figure 7. Since tangential stresses linearly vary along depth in the yielded portion of the interface (Figure 4(a)), n is imposed equal to 2/3.

4. Model validation

The model predictions are compared with the numerical results of the reference case (Tables 1 and 2, for both $\delta = 0$ and 20°) in Figure 11. For the sake of completeness, the results are compared in the $U_{t,diff}$-H, $U_{t,av}$-H, $U_{b,f}$-H and Σ_f-H planes (Figure 11(a–d), respectively). As is evident, the agreement is quite satisfactory. Only in case of differential settlements the model predictions are slightly less accurate, but the agreement in terms of H^* values is very satisfactory. The importance of this observation will be clarified in Section 5.

To further validate the proposed model, the authors compared the model results with the data of a parametric study, by starting from the reference case (Tables 1 and 2) and by considering different δ, L and S values. The results in terms of h^* ($h^* = H^*d$) and dimensional average displacements at the embankment top ($u_{t,av}$) are plotted in Figure 12. For all the cases considered the agreement is satisfactory.

5. Practical application

5.1. General comments

From a practical point of view, the designers may be interested in having a quantitative estimation of the influence of pile shaft friction on the settlement development.

As was observed in Section 2.1, for sufficiently large values of H ($H > H^*$), all the $U_{t,av}$-H and $U_{t,diff}$-H curves become parallel (for fixed S, L, $E_{oed,e}/E_{oed,f}$, ϕ'_e and ψ_e), independently on the δ value. This implies that for $H > H^*$ the incremental system stiffness (C_{av}^{-1} and C_{diff}^{-1}) is not affected by pile shaft friction. This is particularly interesting from a practical point of view: if a designer intends to analyse the embankment response to perturbation imposed after the end of the construction process (Section 5.2), the pile shaft roughness can completely be disregarded if $H > H^*$.

On the contrary, for $H < H^*$ the slope of both $U_{t,av}$-H and $U_{t,diff}$-H curves is severely influenced by the pile shaft roughness. To put in evidence such a dependency, the variation in the C_{av} initial value ($C_{av,0}$), representing the initial slope of the $U_{t,av}$-H curve, with geometry (S and L) and δ, obtained by employing the generalized constitutive relationship described in Section 3, is reported in Figure 13.

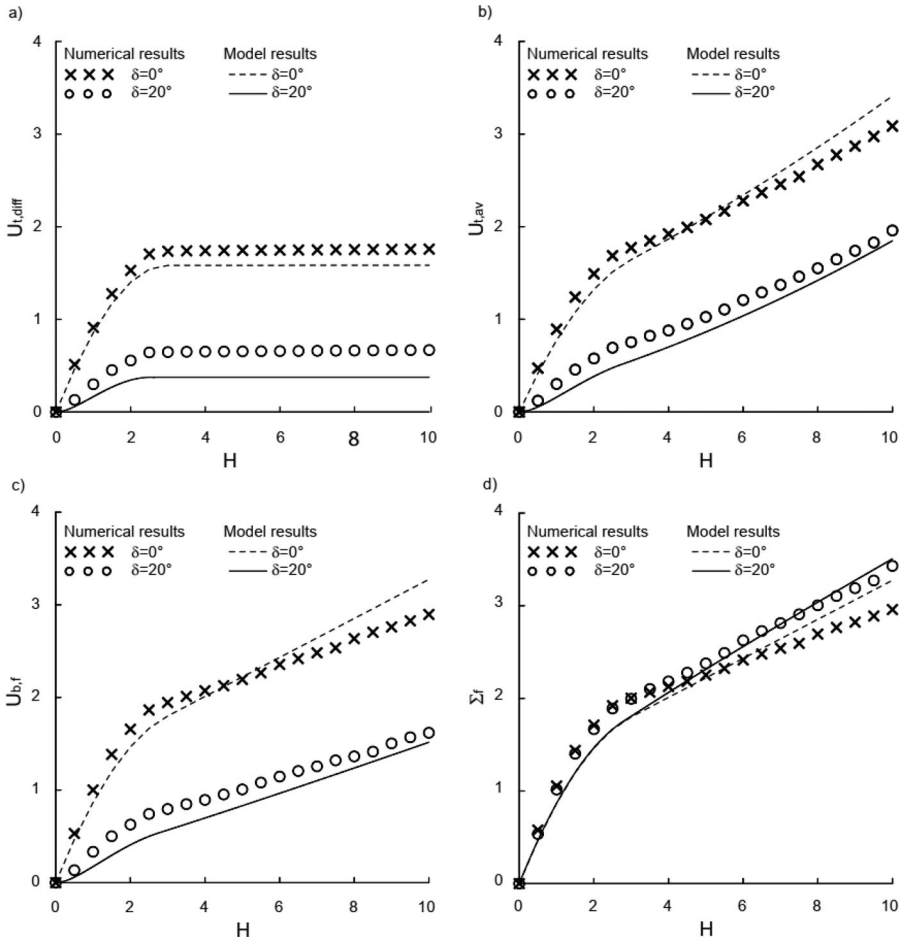

Figure 11. Validation of the model on the results of the reference case: (a) $U_{t,diff}$-H, (b) $U_{t,av}$-H, (c) $U_{b,f}$-H and (d) Σ_f-H planes.

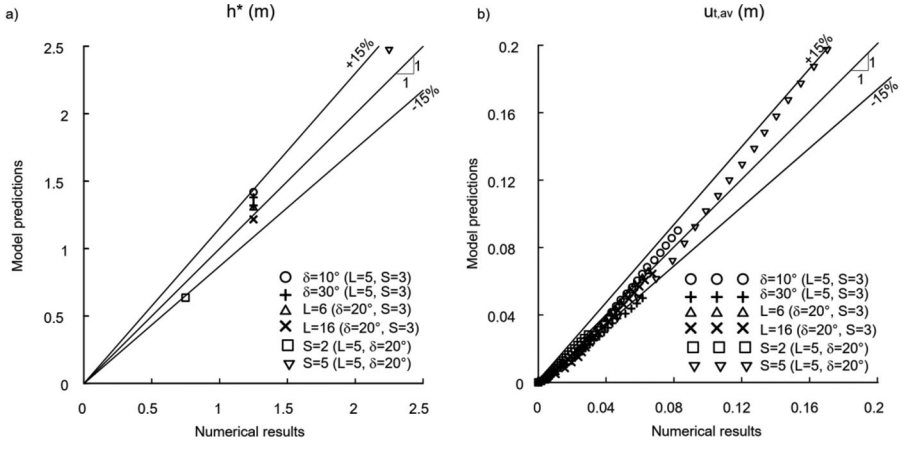

Figure 12. Validation of the model on the results of a parametric study.

As was expected, the influence of the pile shaft roughness on $C_{av,0}$ is more pronounced for small spacing values (Figure 13(a)) and for long piles (Figure 13(b)). An almost coincident trend is obtained for the initial value of C_{diff}, but the corresponding results are hereafter omitted for the sake of brevity. On the

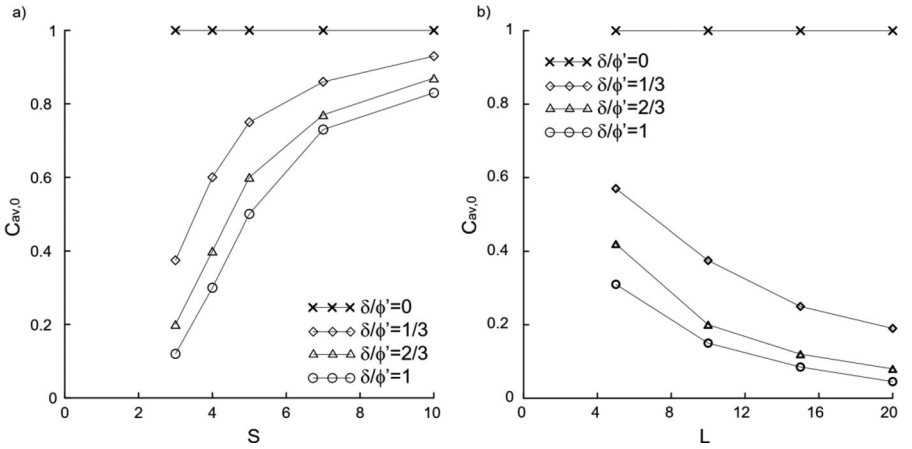

Figure 13. (a) Influence of S and δ on $C_{av,0}$ (L = 10) and (b) influence of L and δ on $C_{av,0}$ (S = 3).

contrary, this influence is small for very large spacing values ($S > 10$) and very short piles ($L < 5$), cases these latter not realistic in practical applications.

5.2. Guided model employment

The model proposed in the previous section can be employed not only to estimate settlements developing during the embankment construction, but also the system response when the top of the embankment is perturbed by uniformly distributed exercise loads (e.g. in case either a ballast for railways or asphalt layers for roads are laid over the embankment top). To exemplify this, the model is employed as a preliminary design tool in relation to the construction of a 2 m thick embankment, on the top of which 30 cm of railway ballast is laid.

The embankment is assumed to be positioned above a 10 m thick soft soil stratum. The foundation soil and the embankment mechanical properties are enlisted in Table 4. The ballast mechanical properties and unit weight are assumed to be coincident with the ones of the embankment. For the sake of simplicity, in the proposed model the ballast positioning is interpreted as an increment in the embankment height.

Hereafter, the following design constraints are imposed:

i. nil differential displacements at the embankment top due to the ballast construction;
ii. an admissible average displacements at the embankment top due to the ballast construction ($\Delta u_{t,adm}$) equal to 2 mm.

As is evident, to satisfy constraint (i) an embankment without piles can be built. However, without piles the increment in dimensional average displacements at the embankment top induced by the ballast construction ($\Delta u_{t,av}$), is equal to:

$$\Delta u_{t,av} = \left(\frac{I}{E_{oed,f}} + \frac{h_e}{E_{oed,e}}\right)\gamma_b h_b = 4cm > \Delta u_{t,adm}, \tag{30}$$

being γ_b and h_b the ballast unit weight and thickness. Since $\Delta u_{t,av}$ is not admissible, piles must be employed to reduce settlements.

For the sake of simplicity, the pile diameter has been imposed and the only design variable will be the pile spacing. Here in the following the case $d = 0.5$ m is discussed.

Constraint (i), corresponding to condition $C_{diff} = 0$, is satisfied if the final embankment height is equal or larger than the height of the plane of equal settlements ($h_e/d = H_e \geq H^*$).

When $\delta > 0$, C_{diff} (Equation (28)) is a function of both input data (geometry and material mechanical properties) and hardening variables (H_{pe}, H_{pf} and Σ_f). For this reason, the H^* value is estimated by

Table 4. Mechanical properties.

$E_{oed,e}$ [MPa]	ϕ'_e [°]	ψ_e [°]	γ_e [kN/m^3]	$E_{oed,f}$ [MPa]	γ_f [kN/m^3]	δ [°]
65	40	0	18	1.35	15	20

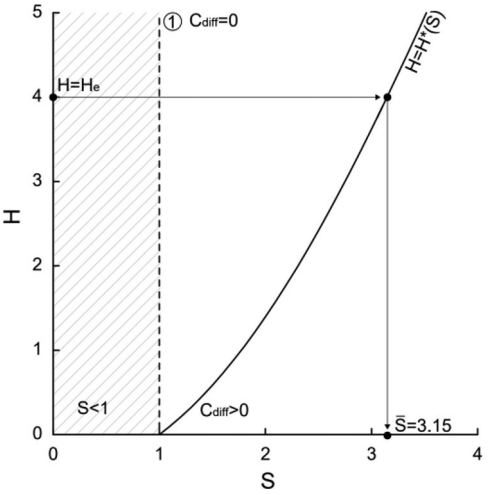

Figure 14. Variation of H^* with S.

integrating the constitutive relationship. For practical purposes, since H^* is not significantly affected by the δ value (Figure 2(a)), the analytical expression obtained in di Prisco et al. (2020a) for $\delta = 0$, derived by imposing $C_{diff} = 0$:

$$H^* = \frac{1}{2}\sqrt{\left(\frac{E_{oed,f}}{E_{oed,e}}\frac{L}{S^2}\right)^2 + \left(\frac{E_{oed,f}}{E_{oed,e}}\frac{L}{S^2}\right)\frac{(S^2-1)}{\overline{k}_e \tan\phi'_{ss}}} - \frac{1}{2}\left(\frac{E_{oed,f}}{E_{oed,e}}\frac{L}{S^2}\right), \tag{31}$$

can be employed. The curve corresponding to Equation $H = H^*$ for $d = 0.5$ m, $l = 10$ m, mechanical properties of Table 4 and varying S values is plotted in Figure 13.

The value of $S = \overline{S}$ is the one corresponding to $H = H_e = H^*$. $\overline{S}$ is the maximum spacing value associated with $C_{diff} = 0$. This condition is satisfied everywhere in subdomain 1 of Figure 14 ranging from the vertical straight line $S = 1$ and function $H = H^*(S)$.

By introducing $\overline{S}$ into the generalized constitutive relationship (Equation (8)), the increment in non-dimensional average displacement ($\Delta U_{t,av}$) associated with the ballast construction can be calculated. The corresponding increment in dimensional displacement:

$$\Delta u_{t,av} = \Delta U_{t,av}\frac{l\gamma_e}{E_{oed,f}} = 1.1mm < \Delta u_{t,adm} \tag{32}$$

is admissible.

In case the average displacement increment was not admissible, a smaller S value should be chosen. As is evident (Figure 14), H^* decreases by decreasing S, meaning that the condition $H_e > H^*$ is satisfied.

In general, also the pile diameter is a design variable. Different d, therefore different L values, corresponding to different functions $H^*(S)$ (Equation (31)), are associated with both different H_e and $\overline{S}$ values. For a given system performance (in this case constraints (i) and (ii)), multiple combinations of d and s can be obtained. For optimizing the design, a suitable cost definition has to be chosen as a function of both in-situ conditions and technological construction constraints. For the sake of generality, this aspect is here not addressed.

6. Concluding remarks

In this paper, by performing a series of 3D finite difference numerical analyses simulating a drained layer-by-layer embankment construction, the authors analyse the mechanical response of embankment founded on piles, whose tip gets a rigid bedrock. In particular, the role of pile shaft roughness is taken into account.

The numerical results put in evidence that (i) owing to the embankment deformability, independently of the pile shaft roughness, a 'complete' arching mechanism, completely deviating vertical stress increments toward the pile, does not develop and (ii) the pile shaft roughness reduces settlements at both embankment top and base but does not significantly affect the height of the plane of equal settlements.

The final goal of this paper is the introduction of a displacement-based design numerical tool, useful to optimize at the pre-design stage, the system geometry (pile diameter and spacing). To this aim, a generalized constitutive relationship, capable of assessing, once geometry and mechanical properties are assigned, both average and differential settlements induced by the embankment construction, has been proposed. The constitutive relationship, based on both a substructuring of the spatial domain and the concept of plane of equal settlements, is conceived and calibrated on the basis of the previously mentioned finite difference results. The numerical tool has been validated by employing these results and its reliability has been shown. Its practical application has proven the simplicity of its use.

The model proposed by the authors is conceived by considering axisymmetric conditions and, therefore, can only be applied for piles belonging to the central part of the embankment. Moreover, the model here proposed considers end bearing piles but can also be extended to the case of 'floating piles' by adding elements to the upscaled constitutive model.

Acknowledgements

All the numerical results have been obtained by using the commercial code FLAC3D^{TM} within the framework of the Itasca Education Partnership (IEP) program. The authors would like to acknowledge Itasca Consulting Group and Harpaceas, collectively providing the software licence.

References

Abdullah, C. H., & Edil, T. B. (2007). Numerical analysis of catenary load transfer platform for geopier-supported embankment. In: Don J. DeGroot, Cumaraswamy Vipulanandan, Jerry A. Yamamuro, Victor N. Kaliakin, Poul V. Lade, Mourad Zeghal, Usama El Shamy, Ning Lu, Chung R. Song Denver, (Eds.), *Advances in measurement and modeling of soil behavior* (pp. 1–10). American Society of Civil Engineers, Colorado, United States. https://doi.org/10.1061/40917(236)11.

Ambily, A. P., & Gandhi, S. R. (2007). Behavior of stone columns based on experimental and FEM analysis. *Journal of Geotechnical and Geoenvironmental Engineering*, *133*(4), 405–415. https://doi.org/10.1061/(ASCE)1090-0241(2007)133:4(405)

Ariyarathne, P., Liyanapathirana, D. S., & Leo, C. J. (2013). Effect of geosynthetic creep on reinforced pile-supported embankment systems. *Geosynthetics International*, *20*(6), 421–435. https://doi.org/10.1680/gein.13.00029

ASIRI. (2012). *Recommandations pour la conception, le dimensionnement, l'exécution et le contrôle de l'amélioration des sols de fondation par inclusions rigides*.

Boschi, K., di Prisco, C., & Flessati, L. (2022). Mechanical behaviour of anchored wire meshes: Numerical analyses and analytical modelling. *Canadian Geotechnical Journal*. Under review.

Boschi, K. di Prisco, C. Flessati, L., Galli, A. & Tomasin, M. (2020) Punching tests on deformable facing structures: numerical analyses and mechanical interpretation, *Lecture Notes in Civil Engineering*, 40, pp. 429-437.

Boschi, K., Flessati, L., di Prisco, C. & Mazzon, N. (2021) Numerical analysis of the mechanical response of anchored wire meshes, *Lecture Notes in Civil Engineering*, 2021, 126, pp. 779–785.

BS8006-1. (2010). *Code of practice for strengthened/reinforced soils and other fills*. British Standards Institution.

Byrne, B. W., & Houlsby, G. T. (2003). Foundations for offshore wind turbines. *Philosophical Transactions of the Royal Society of London. Series A: Mathematical, Physical and Engineering Sciences*, *361*(1813), 2909–2930. https://doi.org/10.1098/rsta.2003.1286

Carlsson, B. (1987). *Reinforced soil, principles for calculation*. Terratema AB (in Swedish).

Cassidy, M. J., Randolph, M. F., & Byrne, B. W. (2006). A plasticity model describing caisson behaviour in clay. *Applied Ocean Research*, *28*(5), 345–358. https://doi.org/10.1016/j.apor.2006.08.005

Chen, R. P., Chen, Y. M., Han, J., & Xu, Z. Z. (2008). A theoretical solution for pile-supported embankments on soft soils under one-dimensional compression. *Canadian Geotechnical Journal*, *45*(5), 611–623. https://doi.org/10.1139/T08-003

Cocchetti, G., di Prisco, C., Galli, A., & Nova, R. (2009). Soil–pipeline interaction along unstable slopes: A coupled three-dimensional approach. Part 1: Theoretical formulation. *Canadian Geotechnical Journal*, *46*(11), 1289–1304. https://doi.org/10.1139/T09-028

Collin, J. G. (2004). *Column supported embankment design considerations*. Paper presented at the Proceedings of the 52nd Annual Geotechnical Engineering Conference, Minneapolis, Minnesota United States, 27 February 2004 (pp. 51–78).

Cremer, C., Pecker, A., & Davenne, L. (2002). Modelling of nonlinear dynamic behaviour of a shallow strip foundation with macro-element. *Journal of Earthquake Engineering*, *6*(2), 175–211. https://doi.org/10.1080/13632460209350414

CUR 226. (2010). *Ontwerprichtlijn paalmatrassystemen* [Design guideline piled embankments] (in Dutch).

Dafalias, Y. F., & Manzari, M. T. (2004). Simple plasticity sand model accounting for fabric change effects. *Journal of Engineering Mechanics*, *130*(6), 622–634. https://doi.org/10.1061/(ASCE)0733-9399(2004)130:6(622)

Das, A. K., & Deb, K. (2018). Experimental and 3D numerical study on time-dependent behavior of stone column–supported embankments. *International Journal of Geomechanics*, *18*(4), 04018011. https://doi.org/10.1061/(ASCE)GM.1943-5622.0001110

Dewoolkar, M. M., Santichaianant, K., & Ko, H. Y. (2007). Centrifuge modeling of granular soil response over active circular trapdoors. *Soils and Foundations*, *47*(5), 931–945. https://doi.org/10.3208/sandf.47.931

di Prisco, C., & Flessati, L. (2021a). A generalized constitutive relationship for undrained soil structure interaction problems. *Lecture Notes in Civil Engineering*, *125*, 398–405.

di Prisco, C., & Flessati, L. (2021b). Progressive failure in elastic-viscoplastic media: from theory to practice. *Géotechnique*, *71*(2), 153–169. https://doi.org/10.1680/jgeot.19.P.045

di Prisco, C., Flessati, L., Frigerio, G., & Galli, A. (2020a). Mathematical modelling of the mechanical response of earth embankments on piled foundations. *Géotechnique*, *70*(9), 755–773. https://doi.org/10.1680/jgeot.18.P.127

di Prisco, C., Flessati, L., Frigerio, G., & Lunardi, P. (2018). A numerical exercise for the definition under undrained conditions of the deep tunnel front characteristic curve. *Acta Geotechnica*, *13* (3), 635–649. https://doi.org/10.1007/s11440-017-0564-y

di Prisco, C., Flessati, L., Galli, A., & Mangraviti, V. (2020b). A simplified approach for the estimation of settlements of earth embankments on piled foundations. *Lecture Notes in Civil Engineering*, *40*, 640–648.

di Prisco, C., Flessati, L., & Porta, D. (2020c). Deep tunnel fronts in cohesive soils under undrained conditions: A displacement-based approach for the design of fibreglass reinforcements. *Acta Geotechnica*, *15* (4), 1013–1030. https://doi.org/10.1007/s11440-019-00840-8

di Prisco, C., Nova, R., & Lanier, J. (1993). A mixed isotropic-kinematic hardening constitutive law for sand. *Modern Approaches to Plasticity*, *1*, 83–124.

di Prisco, C., & Pisanò, F. (2011). An exercise on slope stability and perfect elastoplasticity. *Géotechnique*, *61*(11), 923–934. https://doi.org/10.1680/geot.9.P.040

di Prisco, C., & Vecchiotti, M. (2006). A rheological model for the description of boulder impacts on granular strata. *Géotechnique*, *56*(7), 469–482. https://doi.org/10.1680/geot.2006.56.7.469

Drescher, A., & Detournay, E. (1993). Limit load in translational failure mechanisms for associative and non-associative materials. *Géotechnique*, *43*(3), 443–456. https://doi.org/10.1680/geot.1993.43.3.443

EBGEO. (2010). *Empfehlungen für den Entwurf und die Berechnung von Erdkörpern mit Bewehrungen aus Geokunststoffen e EBGEO* (Vol. 2). German Geotechnical Society (in German).

Flessati, L. (2021). Application of an innovative displacement based design approach for earth embankments on piled foundations. *Lecture Notes in Civil Engineering*, *126*, 293–299.

Flessati, L., & di Prisco, C. (2020). Deep tunnel faces in cohesive soils under undrained conditions: Application of a new design approach. *European Journal of Civil and Environmental Engineering*. In Press. doi.org/10.1080/19648189.2020.1785332

Flessati, L., di Prisco, C., & Callea, F. (2021). Numerical and theoretical analyses of settlements of strip shallow foundations on normally consolidated clays under partially drained conditions. *Géotechnique*, *71*(12), 1114–1134. doi.org/10.1680/jgeot.19.P.348. https://doi.org/10.1680/jgeot.19.P.348

Gottardi, G., Houlsby, G. T., & Butterfield, R. (1999). Plastic response of circular footings on sand under general planar loading. *Géotechnique*, *49*(4), 453–470. https://doi.org/10.1680/geot.1999.49.4.453

Grange, S., Kotronis, P., & Mazars, J. (2009). A macro-element to simulate dynamic soil-structure interaction. *Engineering Structures*, *31*(12), 3034–3046. https://doi.org/10.1016/j.engstruct.2009.08.007

Han, J., & Gabr, M. A. (2002). Numerical analysis of geosynthetic-reinforced and pile-supported earth platforms over soft soil. *Journal of Geotechnical and Geoenvironmental Engineering*, *128*(1), 44–53. https://doi.org/10.1061/(ASCE)1090-0241(2002)128:1(44)

Han, J., Oztoprak, S., Parsons, R. L., & Huang, J. (2007). Numerical analysis of foundation columns to support widening of embankments. *Computers and Geotechnics*, *34*(6), 435–448. https://doi.org/10.1016/j.compgeo.2007.01.006

Handy, R. L. (1985). The arch in soil arching. *Journal of Geotechnical Engineering*, *111*(3), 302–318. https://doi.org/10.1061/(ASCE)0733-9410(1985)111:3(302)

Hewlett, W. J., & Randolph, M. F. (1988). Analysis of piled embankments. In *International journal of rock mechanics and mining sciences and geomechanics abstracts* (Vol. 25, No. 6, pp. 297–298). Elsevier Science.

Huang, J., & Han, J. (2010). Two-dimensional parametric study of geosynthetic-reinforced column-supported embankments by coupled hydraulic and mechanical modeling. *Computers and Geotechnics*, *37*(5), 638–648. https://doi.org/10.1016/j.compgeo.2010.04.002

Iglesia, G. R. (1991). *Trapdoor experiments on the centrifuge - A study of arching in geomaterials and similitude in geotechnical models* [PhD thesis]. Department of Civil Engineering, Massachusetts Institute of Technology.

Iglesia, G. R., Einstein, H. H., & Whitman, R. V. (1999, June). *Determination of vertical loading on underground structures based on an arching evolution concept*. Paper presented at the Proceedings of the 3rd National Conference - Geo-Engineering for Underground Facilities, University of Illinois, Urbana-Champaign, IL (pp. 495–506).

Iglesia, G. R., Einstein, H. H., & Whitman, R. V. (2013). Investigation of soil arching with centrifuge tests. *Journal of Geotechnical & Geoenvironmental Engineering*, *140* (2), 04013005-1 - 04013005-13. https://doi.org/10.1061/(ASCE)GT.1943-5606.0000998.

Itasca Consulting Group Inc. (2017). *FLAC3D—Fast lagrangian analysis of continua in three-dimensions* (Version 7.0). Itasca.

Kempfert, H. G., Göbel, C., Alexiew, D., & Heitz, C. (2004). *German recommendations for reinforced embankments on pile-similar elements*. Paper presented at the EuroGeo3-Third European Geosynthetics Conference, Geotechnical Engineering with Geosynthetics, Deutsche Gesell schaft fur Geotechnik, Munich, Germany (pp. 279–284).

King, D. J., Bouazza, A., Gniel, J. R., Rowe, R. K., & Bui, H. H. (2017). Serviceability design for geosynthetic reinforced column supported embankments. *Geotextiles and Geomembranes*, *45*(4), 261–279. https://doi.org/10.1016/j.geotexmem.2017.02.006

Ladanyi, B., & Hoyaux, B. (1969). A study of the trap-door problem in a granular mass. *Canadian Geotechnical Journal*, *6*(1), 1–14. https://doi.org/10.1139/t69-001

Lehn, J., Moormann, C., & Aschrafi, J. (2016). Numerical investigations on the load distribution over the geogrid of a basal reinforced piled embankment under cyclic loading. *Procedia Engineering*, *143*, 435–444. https://doi.org/10.1016/j.proeng.2016.06.055

Li, Z., Kotronis, P., Escoffier, S., & Tamagnini, C. (2016). A hypoplastic macroelement for single vertical piles in sand subject to three-dimensional loading conditions. *Acta Geotechnica*, *11*(2), 373–390. https://doi.org/10.1007/s11440-015-0415-7

Liu, H. L., Ng, C. W., & Fei, K. (2007). Performance of a geogrid-reinforced and pile-supported highway embankment over soft clay: Case study. *Journal of Geotechnical and Geoenvironmental Engineering*, *133*(12), 1483–1493. https://doi.org/10.1061/(ASCE)1090-0241(2007)133:12(1483)

Mangraviti, V., Flessati, L., & di Prisco, C. (2021). Modelling the development of settlements of earth embankments on piled foundations. *Lecture Notes in Civil Engineering*, *126*, 811–816.

Manzari, M. T., & Dafalias, Y. F. (1997). A critical state two-surface plasticity model for sands. *Géotechnique*, *47*(2), 255–272. https://doi.org/10.1680/geot.1997.47.2.255

Marveggio, P., Redaelli I., & di Prisco C. (2022). Phase transition in monodisperse granular materials: how to model it by using a strain hardening visco-elastic-plastic constitutive relationship. *International Journal for Numerical and Analytical Methods in Geomechanics*. Under review.

Marston, A., & Anderson, A. O. (1913). *The theory of loads on pipes in ditches and tests on cement and clay drain tile and sewer pipe*. Bullettin No. 31. Engineering Experiment Station.

Martin, C. M., & Houlsby, G. T. (2001). Combined loading of spudcan foundations on clay: Numerical modelling. *Géotechnique*, *51*(8), 687–699. https://doi.org/10.1680/geot.2001.51.8.687

McGuire, M. P. (2011). *Critical height and surface deformation of column-supported embankments* [PhD thesis]. Department of Civil Engineering, Virginia Polytechnic Institute and State University.

McKelvey, J. A, III. (1994). The anatomy of soil arching. *Geotextiles and Geomembranes*, *13*(5), 317–329. https://doi.org/10.1016/0266-1144(94)90026-4

Montrasio, L., & Nova, R. (1997). Settlements of shallow foundations on sand: Geometrical effects. *Géotechnique*, *47*(1), 49–60. https://doi.org/10.1680/geot.1997.47.1.49

Naughton, P. J. (2007). *The significance of critical height in the design of piled embankments*. In Soil Improvement (pp. 1–10). https://doi.org/10.1061/40916(235)3

Nova, R., & Montrasio, L. (1991). Settlements of shallow foundations on sand. *Géotechnique*, *41*(2), 243–256. https://doi.org/10.1680/geot.1991.41.2.243

Pisanò, F., Flessati, L., & di Prisco, C. (2016). A macroelement framework for shallow foundations including changes in configuration. *Géotechnique*, *66*(11), 910–926. https://doi.org/10.1680/jgeot.16.P.014

Plaut, R. H., & Filz, G. M. (2010). Analysis of geosynthetic reinforcement in pilesupported embankments. Part III: Axisymmetric model. *Geosynthetics International*, *17*(2), 77–85. [https://doi.org/10.1680/gein.2010.17.2.77]

Rogbeck, Y., Gustavsson, S., Sodergren, I., & Lindquist, D. (1998). *Reinforced piled embankments in Sweden-design aspects*. Paper presented at the Proceedings, Sixth International Conference on Geosynthetics (Vol. 2, pp. 755–762).

Russell, D., & Pierpoint, N. (1997). An assessment of design methods for piled embankments. *Ground Engineering*, *30*(10), 39–44.

Stewart, M. E., & Filz, G. M. (2005). Influence of clay compressibility on geosynthetic loads in bridging layers for column-supported embankments. *Contemporary Issues in Foundation Engineering*, *1*, 1–14.

Svanø, G., Ilstad, T., Eiksund, G., & Want, A. (2000). *Alternative calculation principle for design of piled embankments with base reinforcement*. Paper presented at the Proceedings of the 4th Conference of the GIGS, Helsinki, Finland, June 7–9, 2000.

Terzaghi, K. (1936). *Stress distribution in dry and in saturated sand above a yielding trap-door*. Paper presented at the Proceedings of the International Conference of Soil Mechanics, Harvard University, Cambridge, MA (pp. 307–311).

Terzaghi, K. (1943). *Theoretical soil mechanics*. Chapman and Hali, Limited John Wiler and Sons, Inc.

Van Eekelen, S. V., Bezuijen, A., & Van Tol, A. F. (2011). Analysis and modification of the British Standard BS8006 for the design of piled embankments. *Geotextiles and Geomembranes*, *29*(3), 345–359. https://doi.org/10.1016/j.geotexmem.2011.02.001

Van Eekelen, S. J. M., Bezuijen, A., & Van Tol, A. F. (2013). An analytical model for arching in piled embankments. *Geotextiles and Geomembranes*, *39*, 78–102. https://doi.org/10.1016/j.geotexmem.2013.07.005

Vardoulakis, I., Graf, B., & Gudehus, G. (1981). Trap-door problem with dry sand: A statical approach based upon model test kinematics. *International Journal for Numerical and Analytical Methods in Geomechanics*, *5* (1), 57–78. https://doi.org/10.1002/nag.1610050106

Vermeer, P. A. (1990). The orientation of shear bands in biaxial tests. *Géotechnique*, *40*(2), 223–236. https://doi.org/10.1680/geot.1990.40.2.223

Wijerathna, M., & Liyanapathirana, D. S. (2020). Load transfer mechanism in geosynthetic reinforced column-supported embankments. *Geosynthetics International*, *27*(3), 236–248. https://doi.org/10.1680/jgein.19.00022

Yan, L., Yang, J. S., & Han, J. (2006). Parametric study on geosynthetic-reinforced pile-supported embankments. In *Advances in earth structures: Research to practice* (pp. 255-261). https://doi.org/10.1061/40863(195)28

Yapage, N. N. S., & Liyanapathirana, D. S. (2014). A parametric study of geosynthetic-reinforced column-supported embankments. *Geosynthetics International*, *21*(3), 213–232. https://doi.org/10.1680/gein.14.00010

Zaeske, D. (2001). *Zur Wirkungsweise von unbewehrten und bewehrten mineralischen Tragschichten über pfahlartigen Gründungselementen*. Fachgebiet u. Versuchsanst. Geotechnik.

Zheng, G., Yang, X., Zhou, H., & Chai, J. (2019). Numerical modeling of progressive failure of rigid piles under embankment load. *Canadian Geotechnical Journal*, *56*(1), 23–34. https://doi.org/10.1139/cgj-2017-0613

Zhuang, Y., Cheng, X., & Wang, K. (2020). Analytical solution for geogrid-reinforced piled embankments under traffic loads. *Geosynthetics International*, *27*(3), 249–260. https://doi.org/10.1680/jgein.19.00023

Appendix A

According to the rheological scheme of Figure 7:

$$\dot{U}_{t,f} = C_{e,2}\dot{H} + (C_{e,1} + C_{f,1})\dot{\Sigma}_f + C_{f,2}\dot{\Sigma}_{f,2} + C_{f,3}\dot{\Sigma}_{f,3}, \tag{A1}$$

$$\dot{U}_{t,c} = C_{e,2}\dot{H} + C_{e,1}\dot{\Sigma}_c, \tag{A2}$$

being

$$\dot{\Sigma}_f = \dot{H} - \frac{4\dot{\mathcal{T}}_{p,e}}{\pi(S^2-1)} = \left(1 - \frac{4\bar{k}_e \tan\phi'_{ss} H_{p,e}}{(S^2-1)}\right)\dot{H}, \tag{A3}$$

$$\dot{\Sigma}_c = \dot{H} + \frac{4\dot{\mathcal{T}}_{p,e}}{\pi} = \left(1 + 4\bar{k}_e \tan\phi'_{ss} H_{p,e}\right)\dot{H}, \tag{A4}$$

$$\dot{\Sigma}_{f,2} = \left\langle \dot{\Sigma}_f - \frac{4\dot{\mathcal{T}}_{p,f}}{\pi(S^2-1)} \right\rangle, \tag{A5}$$

$$\dot{\Sigma}_{f,3} = \left\langle \dot{\Sigma}_f - \frac{4\left(\dot{\mathcal{T}}_{p,f} + \dot{\mathcal{T}}_{e,f}\right)}{\pi(S^2-1)} \right\rangle, \tag{A6}$$

where the Macaulay brackets, ensuring $\dot{\Sigma}_{f,2}$ and $\dot{\Sigma}_{f,3}$ to be positive, are introduced to ensure the force increment globally transferred ($\dot{\mathcal{T}}_{p,f}$ and $\dot{\mathcal{T}}_{e,f}$) by arching in the foundation soil not to exceed $\dot{\Sigma}_f$.

By introducing Equations (A1) and (A2) into Equations (2) and (3) it reads:

$$\dot{U}_{t,diff} = C_{e,1}\left(\dot{\Sigma}_f - \dot{\Sigma}_c\right) + C_{f,1}\dot{\Sigma}_f + C_{f,2}\dot{\Sigma}_{f,2} + C_{f,3}\dot{\Sigma}_{f,3}, \tag{A7}$$

$$\dot{U}_{t,av} = C_{e,2}\dot{H} + \frac{C_{e,1}}{S^2}\left[(S^2-1)\dot{\Sigma}_f + \dot{\Sigma}_c\right] + \frac{\left(C_{f,1}\dot{\Sigma}_f + C_{f,2}\dot{\Sigma}_{f,2} + C_{f,3}\dot{\Sigma}_{f,3}\right)(S^2-1)}{S^2}, \tag{A8}$$

Finally, by substituting Equations (19) (22) (25), and (A3)–(A6) into Equations (A7) and (A8), Equations (28) and (29) are obtained.